Composites Science and Technology 70 (2010) 1057–1063

Contents lists available at ScienceDirect

Composites Science and Technology

journal homepage: www.elsevier.com/locate/compscitech

The transverse elastic properties of chiral honeycombs

A. Lorato [c], P. Innocenti [c], F. Scarpa [c], A. Alderson [b], K.L. Alderson [b,*], K.M. Zied [b], N. Ravirala [b], W. Miller [a], C.W. Smith [a], K.E. Evans [a]

[a] School of Engineering, Computing and Mathematics, University of Exeter, Exeter EX4 4QF, UK
[b] Centre for Materials Research and Innovation, University of Bolton, Deane Road, Bolton BL3 5AB, UK
[c] Department of Aerospace Engineering, University of Bristol, University Walk, Bristol BS8 1TR, UK

ARTICLE INFO

Article history:
Received 8 December 2008
Received in revised form 18 June 2009
Accepted 20 July 2009
Available online 24 July 2009

Keywords:
A. Smart materials
B. Mechanical properties
C. Elastic properties
C. Deformation
C. Finite element analysis

ABSTRACT

This work describes the out-of-plane linear elastic mechanical properties of trichiral, tetrachiral and hexachiral honeycomb configurations. Analytical models are developed to calculate the transverse Young's modulus and the Voigt and Reuss bounds for the transverse shear stiffness. Finite Element models are developed to validate the analytical results, and to identify the dependence of the transverse shear stiffness vs. the gauge thickness of the honeycombs. The models are then validated with experimental results from flatwise compressive and simple shear tests on samples produced with rapid prototype (RP)-based techniques.

1. Introduction

Honeycomb structures are widely used as sandwich panel cores in applications such as aerospace components, due to their excellent density specific properties [1]. However, the design of honeycomb structures has changed little since their introduction over 60 years ago. The requirement for lower mass and cost for components for use in transport applications is becoming increasingly important, and one response to these pressures has been to introduce multi-functionality into existing components [2]. An excellent candidate for this is the redesign of the conventional hexagonal cell geometry of the honeycomb cores in sandwich panels. Current conventional hexagonal geometry honeycomb panels exhibit anticlastic or saddle-shaped curvatures when deformed out of plane [3], consequently current methods of producing dome shaped panels, e.g. by deforming a flat sheet of conventional honeycomb into the desired shape, or by machining a block to the required profile often lead to increased costs or localised damage [3]. The problem of creating domed structures can be overcome if the in-plane Poisson's ratios of a honeycomb are negative (auxetic) due to the change of cell shape from hexagonal to re-entrant bow-tie shapes. In such a case, domed or synclastic bending geometries can be achieved relatively easily, without further machining [4]. Other benefits provided by auxetic honeycombs include an increased in-plane shear modulus and enhanced indentation resistance.

The field of negative Poisson's ratio (auxetic) materials goes beyond just honeycombs and includes crystalline materials [5], foams [6], biomaterials [7] and liquid crystals [8]. For comprehensive reviews see [9–11]. Auxetic behaviour in honeycombs can be achieved via specific cell geometries, including centre-symmetric re-entrant bow tie shaped cells [4,12] which exhibit reflective and rotational symmetry, or by non centre-symmetric chiral cells [13–20], which have rotational symmetry but not reflective symmetry as in conventional honeycombs. However, it is possible to design cell geometries which are non centre-symmetric and are similar to the chiral geometries but which do exhibit reflective symmetry, which will be referred to as 'anti-chiral'. The chiral and anti-chiral geometries are the subject of the present work. In 1989, Wojciechowski [21] suggested for the first time an auxetic chiral configuration based on rotating disks and nearest neighbour inverse nth power interactions. A chiral honeycomb providing a theoretical in-plane Poisson's ratio of -1 was introduced by Prall and Lakes [14].

Chiral cellular solids provide significant advantages over conventional hexagonal honeycombs, the compressive and shear strengths are partially decoupled between the cylinders and the ligaments and both the off axis deformations and the electromagnetic functionality of the honeycomb is tuneable through variation of honeycomb geometry [16,20]. Most previous work on chiral structures has concentrated on interesting and potentially useful in-plane behaviour, but relatively little has been conducted on through thickness behaviour, aside from flatwise compression [15,16] and initial transverse shear in hexagonal honeycomb configurations [22]. However, through-the-thickness properties

---

* Corresponding author. Tel.: +44 01204 903519.
E-mail address: ka1@bolton.ac.uk (K.L. Alderson).

0266-3538/$ - see front matter © 2009 Elsevier Ltd. All rights reserved.
doi:10.1016/j.compscitech.2009.07.008

become important for the multifunctional behaviour of sandwich panels, for example flexural stiffness, energy absorption, resistance to wrinkling, and sound and electromagnetic insulation [1].

This paper presents the through thickness linear elastic behaviour of five chiral based geometry structures, using mechanical characterisation, numerical and analytical modelling. The chiral topologies consist of a hexagonal chiral (hexachiral) with six connectivities, a tetrachiral (four connectivities), and a trichiral (three connectivities). For the tetrachiral and trichiral configurations, it is also possible to identify antitetra and antitrichiral layouts, where the ribs are connected to the same side of the cylinder [23] (see Fig. 1). The linear elastic properties (compressive modulus and shear modulus) are modelled using a combination of analytical and numerical (finite element) techniques, with validation provided by experimental results from flatwise compression and shear tests according to ASTM standards. The through thickness Poisson's ratios are not reported in this work because they are simply determined by the Poisson's ratio of the constituent material and relative density ratios [12] – the honeycombs are not designed to have auxetic behaviour through the thickness.

2. Analytical and numerical models

Fig. 1 shows the overall in-plane layouts of the chiral configurations considered. The cell geometries are defined using a common set of non-dimensional parameters (α, β and γ, where α is L/r, $\beta = t/r$ and $\gamma = b/r$). These are shown in Fig. 2 for a tetrachiral structure. The parameters L, t and r represent the rib length, wall thickness of the node and rib, and radius of the node, respectively. The depth of the cell b is not shown.

The flatwise compressive modulus was calculated analytically, as the ratio between the load bearing area and total area of the unit cell [12]. For the shear loading, the chiral configurations were modelled using the finite element codes ABAQUS [24] and ANSYS [25]. For the ANSYS models, three-dimensional elements SOLID45 with eight nodes, three degrees of freedom and Lagrange interpolation functions were used within a mapped meshed technique to provide three linear elements per minimum dimension of the unit cells. For the trichiral configurations, SHELL63 elements were also used. The minimum size for the elements was identified after a mesh

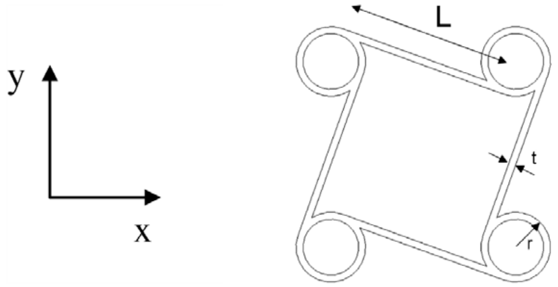

Fig. 2. Diagram of tetrachiral structure showing parameters nomenclature.

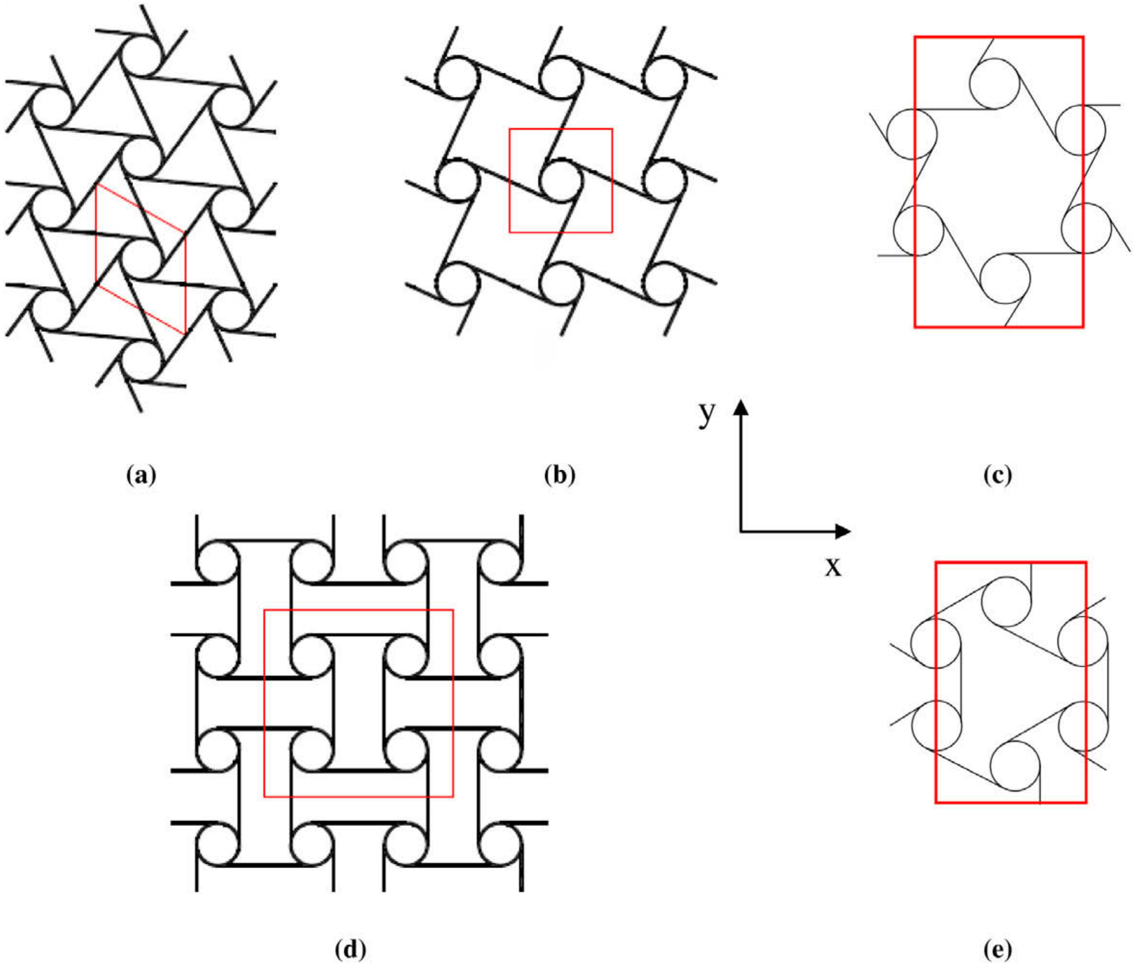

Fig. 1. Cell geometries for the auxetic chiral, anti-chiral, and conventional centre-symmetric and hexagonal structures: (a) hexachiral, (b) tetrachiral, (c) trichiral, (d) anti tetra chiral, and (e) anti tri chiral.

convergence analysis. A similar approach was used with the ABAQUS code, implementing C3D20R 20 node quadratic reduced integration brick elements. The transverse shear loading was simulated applying boundary conditions as devised by Grediac [26]. For the 13 surface loading (Fig. 3), the upper surface of the cell was loaded with an imposed non-zero displacement u along the 1-direction, while restraining the other two degrees of freedom. The lower surface was completely clamped, while the vertical edges were only constrained along the 3-direction. The shear strain γ_{13} was calculated as u/b, where b is the gauge thickness of the honeycomb along the 3-direction. The resulting shear stress τ_{23} was calculated as F/S, where F is the resultant of the shear forces on the upper surface of the cell after solving a linear elastic problem, and S is the area of the chiral cell. The transverse shear modulus was then calculated as the ratio between the shear stress and shear strain.

From a theoretical point of view, the transverse shear modulus of general honeycomb cores is bounded between an upper bound (Voigt), and lower bound (Reuss). The two bounds can be calculated using either unit load and unit displacement methods [17], or the theorems of minimum strain energy and minimum complementary strain energy [16]. It is possible to determine closed form solutions for the Voigt bounds, while the Reuss can be determined by solving a non-linear minimisation problem. A unique value for the transverse shear can be identified through an interpolation between the bounds based on the effect of the gauge thickness of the honeycomb over the shear stress distributions in the cell [17].

2.1. Compressive modulus

The compressive modulus of a honeycomb structure can be calculated considering the density of the cellular solid itself [20]:

$$\frac{E_z}{E_{core}} = \frac{\rho}{\rho_{core}} \tag{1}$$

where E_{core} and ρ_{core} are the modulus and density of the solid material.

Considering the non-dimensional geometry parameters of the unit cells, and a uniform thickness for both the ribs and the nodes, the load bearing area of a node, A_{node}, is:

$$A_{node} = \pi r^2 \beta (2-\beta) \tag{2}$$

and the area of a rib, A_{rib}, is:

$$A_{rib} = \alpha \beta r^2 \tag{3}$$

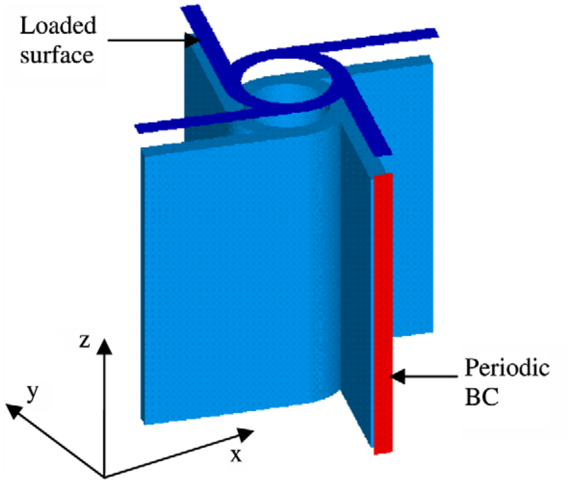

Fig. 3. Tetrachiral unit cell with BC under shear. Top – loaded surface. Side (red) – periodic BC shear conditions (for interpretation of the references to colour in this figure legend, the reader is referred to the web version of this article).

For honeycombs where the thickness of the ribs and nodes cannot be neglected it is necessary to consider the area of overlap, A_{junc}, at the junction between a node and rib. This is given by the area of segment AOC minus the area of triangle BOC in Fig. 4:

$$A_{junc} = \frac{r^2}{2}[\phi - (1-\beta)\sin\phi] \tag{4}$$

where $\varphi = \cos^{-1}(1-\beta)$.

The relative density of each honeycomb is then given by the ratio of the area of solid material, A_{core}, within a representative unit cell to the area of the unit cell, A_{u-c}:

$$\frac{\rho}{\rho_{core}} = \frac{A_{core}}{A_{u-c}} = \frac{n_{rib}A_{rib} + n_{node}A_{node} - n_{junc}A_{junc}}{A_{u-c}} \tag{5}$$

where n_{rib}, n_{node} and n_{junc} are the numbers of ribs, nodes and junctions, respectively, in the unit cell. The areas of the unit cells (shown as boxes) in Fig. 1 are

$$A_{hex} = 2\sqrt{3}r^2\left(\left(1-\frac{\beta}{2}\right)^2 + \frac{\alpha^2}{4}\right) \tag{6a}$$

$$A_{tetra} = 4r^2\left(\left(1-\frac{\beta}{2}\right)^2 + \frac{\alpha^2}{4}\right) \tag{6b}$$

$$A_{antitetra} = 4r^2\alpha^2 \tag{6c}$$

$$A_{tri} = 12\sqrt{3}r^2\left(\left(1-\frac{\beta}{2}\right)^2 + \frac{\alpha^2}{4}\right) \tag{6d}$$

$$A_{antitri} = 3\sqrt{3}r^2\alpha^2 \tag{6e}$$

From Eqs. (2)–(5), (6a)–(6e) the following expressions for the density ratios of the chiral and anti-chiral honeycomb configurations are obtained:

$$\left.\frac{\rho}{\rho_{core}}\right|_{hexa} = \frac{\beta[3\alpha + \pi(2-\beta)] - 3[\phi - (1-\beta)\sin\phi]}{2\sqrt{3}\left[\left(1-\frac{\beta}{2}\right)^2 + \frac{\alpha^2}{4}\right]} \tag{7a}$$

$$\left.\frac{\rho}{\rho_{core}}\right|_{tetra} = \frac{\beta[2\alpha + \pi(2-\beta)] - 2[\phi - (1-\beta)\sin\phi]}{4\left[\left(1-\frac{\beta}{2}\right)^2 + \frac{\alpha^2}{4}\right]} \tag{7b}$$

$$\left.\frac{\rho}{\rho_{core}}\right|_{antitetra} = \frac{\beta[2\alpha + \pi(2-\beta)] - 2[\phi - (1-\beta)\sin\phi]}{\alpha^2} \tag{7c}$$

$$\left.\frac{\rho}{\rho_{core}}\right|_{tri} = \frac{\beta[3\alpha + 2\pi(2-\beta)] - 3[\phi - (1-\beta)\sin\phi]}{6\sqrt{3}\left[\left(1-\frac{\beta}{2}\right)^2 + \frac{\alpha^2}{4}\right]} \tag{7d}$$

$$\left.\frac{\rho}{\rho_{core}}\right|_{antitri} = \frac{2\beta[3\alpha + 2\pi(2-\beta)] - 6[\phi - (1-\beta)\sin\phi]}{3\sqrt{3}\alpha^2} \tag{7e}$$

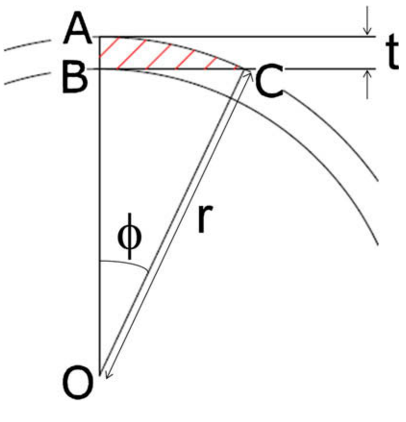

Fig. 4. Rib-node junction.

The compressive modulus for each configuration was then predicted by substituting the relevant equation from (7a) to (7e) into Eq. (1).

2.2. Transverse shear

The upper limit of the transverse shear modulus can be evaluated using the theorem of minimum potential energy [17] which, for a general honeycomb configuration loaded with a uniform strain on the 13 plane, can be stated as:

$$\frac{1}{2}G_{13}\gamma_{13}^2 V \leqslant \frac{1}{2}\sum_i \left(G_{core}\gamma_i^2 V_i\right) \tag{8}$$

where V_i is a volume component of the unit cell. Considering the hexachiral configuration, the various volumes of the unit cell can be calculated as follows:

$$\begin{cases} dV_{rib1} = dV_{rib2} = dV_{rib3} = t\frac{dl}{2}b \\ dV_{cir} = rtb*d\theta \end{cases} \tag{9}$$

The shear strains in the individual volumes are:

$$\begin{cases} \gamma_{rib1} = \gamma_{13}\cos(-\theta) \\ \gamma_{rib2} = \gamma_{13}\cos\left(-\theta + \frac{\pi}{3}\right) \\ \gamma_{rib3} = \gamma_{13}\cos\left(-\theta + \frac{2\pi}{3}\right) \\ \gamma_{cir} = \gamma_{13}\cos\left(\theta + \frac{\pi}{2}\right) = \gamma_{13}\sin\theta \end{cases} \tag{10}$$

where $\sin\theta = 2r/R$, $\tan\theta = 2r/L$ and R is the centre-to-centre distance between two connected nodes. Inserting (10) and (9) in (8), one obtains:

$$\frac{1}{2}G_{13}\gamma_{13}^2 V \leqslant \frac{G_{core}}{2}\left\{2\int[\gamma_{rib1}]^2 dV_{rib1} + 2\int[\gamma_{rib2}]^2 dV_{rib2} + 2\int[\gamma_{rib3}]^2 dV_{rib3}\right\} + \frac{G_{core}}{2}\int[\gamma_{circ}]^2 dV_{cir} \tag{11}$$

Solving the integrals in (11) and making use of the definitions for the non-dimensional geometry parameters α and β, the Voigt limit for the transverse shear modulus G_{13} is:

$$\frac{G_{13}}{G_{core}} \leqslant \frac{\left\{\left[\cos^2(\theta) + \cos^2\left(-\theta + \frac{\pi}{3}\right) + \cos^2\left(-\theta + \frac{2\pi}{3}\right)\right]\cdot\alpha + \pi\right\}}{2\frac{\sqrt{3}}{\sin^2\theta}}\beta \tag{12}$$

For the tetrachiral configuration, similar geometric considerations lead to the following upper limit:

$$\frac{G_{13}}{G_{core}} \leqslant \frac{\left\{\left[\cos^2(\theta) + \cos^2\left(-\theta + \frac{\pi}{2}\right)\right]\alpha + \pi\right\}}{1+\alpha^2}\beta \tag{13}$$

The Voigt limit for the antitetrachiral is:

$$\frac{G_{13}}{G_{core}} \leqslant \frac{\alpha + \pi}{\alpha^2}\beta \tag{14}$$

The upper limit transverse shear scales linearly with the relative density β, as expected in general honeycomb configurations [16,20]. Due to the hexagonal symmetry of the chiral topologies, the upper limits for the transverse shear modulus G_{23} assume the same formulations as in (14), (13), (12). For the Reuss bound, it is possible to apply the theorem of the minimum of the complementary potential energy, which for a general honeycomb configuration loaded in shear over the 13 plane assumes the following form:

$$\frac{1}{2}\frac{\tau_{13}^2}{G_{13}}V \leqslant \frac{1}{2}\sum_i\left(\frac{\tau_i^2}{G_{mat}}V_i\right) \tag{15}$$

Considering an external uniform stress τ_{13} applied to the unit cell, the equilibrium of the resultant forces due to shear stress distributions in the volume components gives the following:

$$2t\frac{l}{2}(\tau_{rib1} + \tau_{rib2} + \tau_{rib3}) + 2\pi rt\tau_{cir} = \tau_{13}2\frac{\sqrt{3}r^2}{\sin^2\theta} \tag{16}$$

At the intersection points between ribs and nodes, the equilibrium between the shear stresses provides the following 3 equilibrium equations:

$$\tau_{cir}^{1+} = \tau_{cir}^{1-} + \tau_{rib1} \tag{17a}$$

$$\tau_{cir}^{2+} = \tau_{cir}^{2-} + \tau_{rib2} \tag{17b}$$

$$\tau_{cir}^{3+} = \tau_{cir}^{3-} + \tau_{rib3} \tag{17c}$$

where the sign + and – for the shear stresses in the connecting sections stands for positive (out) and negative (in) flows. The system of Eqs. (15)–(17) is not analytically solvable, because the function $\tau_{cir}(\theta)$ assumes zero values for $\theta = 0$ or $3/2/\pi$ (only bending contribution), and non-zero values for all the other cases.

It must be noticed that, for isotropic centresymmetric regular hexagonal structures, the upper and lower bounds do coincide [20,21]. Although hexachiral, tetrachiral and trichiral honeycombs are in-plane isotropic, two different bounds exist.

3. Manufacturing and testing

Samples of chiral honeycombs were produced using a Rapid Prototyping (RP) FDM Stratasys machine (Stratasys Inc., USA), using ABS plastics, and a SLS machine (3D Systems Corp, USA) with a combination of geometric parameters as indicated in Tables 1 and 2. The FDM samples had a lower relative density β compared to the SLS samples. For all the RP models, the ABS plastics used had a Young's modulus of 1.0 GPa measured from a tensile test according to the ASTM D6738 standard, while the SLS core material had a Young's modulus of 1.6 GPa. The honeycomb samples had overall front dimensions of 225 × 220 mm, and variable gauge thickness according to the non-dimensional height specified in Table 1.

The flatwise compressive tests were performed according to the ASTM standard C-393 – 00. The hexachiral and tetrachiral samples were subjected to a constant displacement rate of 0.5 mm min^{-1}, with the maximum load occurring between 3 and 6 min. The load was distributed through self-aligned plates, taking care to distribute the deformation in the most uniform way to avoid failure occurring solely at the edges. The trichiral samples were tested at a strain rate of 1 mm min^{-1} with the maximum strain being 3%.

For the shear tests, the SLS and FDM hexachiral and tetrachiral samples were attached to steel plates using a two-part epoxy glue Redux 810, with nominal tensile lap shear strength of 43 MPa. The samples were cured for 5 days at 22 °C, and then attached to an Instron 1342 servohydraulic test machine with 100 kN load cell. The fixtures for the samples were custom designed based on the ASTM C 273-00 standard. The samples were loaded in shear under displacement control with a video-extensometer at a rate of 0.5 mm s^{-1}. The force–displacement curves were post-processed to obtain the shear stress and strain as indicated in the ASTM C 273-00 standard. An analogous setup was designed for the trichiral and antitrichiral FDM samples, using also in this case an Instron 1342 machine with the same technical specifications used for the hexachiral and tetrachiral honeycombs. The shear strain rate used in this case was 1 mm min^{-1}.

4. Results and discussion

Table 2 provides a comparison between the analytical and experimental values of the chiral configurations considered for the flatwise compressive tests. The analytical solutions overestimate the results from the flatwise compressive tests. From visual inspection, it appears that during the compressive loading, the

Table 1
Comparison of numerical and experimental results for shear testing.

	Sample geometry	FE (MPa)	Experimental (MPa)
Antitetrachiral SLS sample 1	$r = 4$ mm $\alpha = 5.4$ $\beta = 0.5$ $\gamma = 6.3$	48.4	52.5
Antitetrachiral SLS sample 2	$r = 4.25$ mm $\alpha = 6.2$ $\beta = 0.35$ $\gamma = 11.8$	44.8	50.2
Tetrachiral FDM	$r = 5$ mm $\alpha = 5.0$ $\beta = 0.12$ $\gamma = 10$	7.9	8.5
Hexachiral FDM	$r = 6$ mm $\alpha = 4$ $\beta = 0.10$ $\gamma = 5.9$	10.1	11.8
Trichiral SLS Sample 1	$r = 5$ mm $\alpha = 5$ $\beta = 0.30$ $\gamma = 2$	15.5	16.3
Trichiral SLS Sample 2	$r = 5$ mm $\alpha = 4$ $\beta = 0.40$ $\gamma = 2$	28.1	22.7
Antitrichiral SLS Sample 1	$r = 5$ mm $\alpha = 5$ $\beta = 0.30$ $\gamma = 2$	15.0	14.9
Antitrichiral SLS Sample 2	$r = 5$ mm $\alpha = 4$ $\beta = 0.40$ $\gamma = 2$	25.3	18.9

Table 2
Comparison between experimental and analytical compressive modulus ($r = 5$ mm).

Cell geometry	Dimensions (mm)	Experimental (MPa)	Analytical (MPa)
Antitetrachiral	$L = 25$, $t = 1.5$, $d = 25$	108.9	160.4
Tetrachiral	$L = 25$, $t = 1.5$, $d = 25$	73.7	143.8
Hexachiral	$L = 25$, $t = 1.5$, $d = 25$	113.4	215.9
Antitetrachiral	$L = 20$, $t = 2$, $d = 25$	183.3	269.8
Tetrachiral	$L = 20$, $t = 2$, $d = 25$	134.9	232.5
Hexachiral	$L = 20$, $t = 2$, $d = 25$	180.7	340.2
Trichiral	$L = 25$, $t = 1.5$, $d = 25$	50.8	94.1
Trichiral	$L = 20$, $t = 2$, $d = 25$	120.4	155.1
Antitrichiral	$L = 25$, $t = 1.5$, $d = 25$	67.6	105.0
Antitrichiral	$L = 20$, $t = 2$, $d = 25$	141.8	179.9

combination of the edge deflection and the finite size of the samples induce some significant rotation effects and lateral movement of the honeycombs. Moreover, the analytical models prescribe a clamped base for the unit cells, providing a further stiffening effect, which is not present in the real experimental situation and these effects could account for the mismatch seen in Table 2. However, the models do capture well the dependency of the compressive modulus vs. the honeycomb configuration. This is particularly true when comparing the results for $\alpha = 5$ and $\beta = 0.3$ (i.e. $L = 25$ mm, $t = 1.5$ mm and $r = 5$ mm), where the modulus increases according to the following order: trichiral → antitrichiral → tetrachiral → antitetrachiral → hexachiral. This trend is consistent with the rib and node number densities increasing with increasing coordination number (from 3- to 4- to 6-ribs per node), and the antichirals displaying a lower cross-sectional area for the same area of solid material with respect to their chiral equivalents. The analytical predictions for $\alpha = 4$ and $\beta = 0.4$ (i.e. $L = 20$ mm, $t = 2$ mm and $r = 5$ mm) also follow the aforementioned trend, although the experimental data show the ordering of the antitrichiral (3-connectivity) and tetrachiral (4-connectivity) honeycombs is reversed, as is that for the antitetrachiral (4-connectivity) and hexachiral (6-connectivity) honeycombs.

For the shear modulus, the hexachiral topologies provide an higher Voigt bound compared to the two tetrachiral ones (Fig. 5), with the hexachiral configuration showing a quasi uniform increase by 42% compared to the tetra and antitetrachiral configurations from aspect ratios α starting from 6. The tetrachiral configurations outperform the hexachiral layout only for α lower than three, with the antitetrachiral providing an higher Voigt bound (33%) compared to the one for the hexagonal chiral honeycomb for $\alpha = 2$. Fig. 6 shows, as an example, the transverse shear values calculated through the FE models for the tetrachiral configurations. The dependence of the shear modulus on gauge thickness ratio γ shows a typical inverse dependence of the type γ^{-1}, as in hexagonal regular [21] and auxetic re-entrant honeycombs [21]. An estimation for the lower (Reuss) bound can be performed considering honeycomb configurations with gauge thickness ratio around 20, with shear modulus almost constant for $\gamma > 17$ for a given set of wall aspect ratios and relative density values. A non-linear least square (NLLS) fitting over 200 configurations of hexachiral and tetrachiral unit cells provides the following estimation for the Reuss bound:

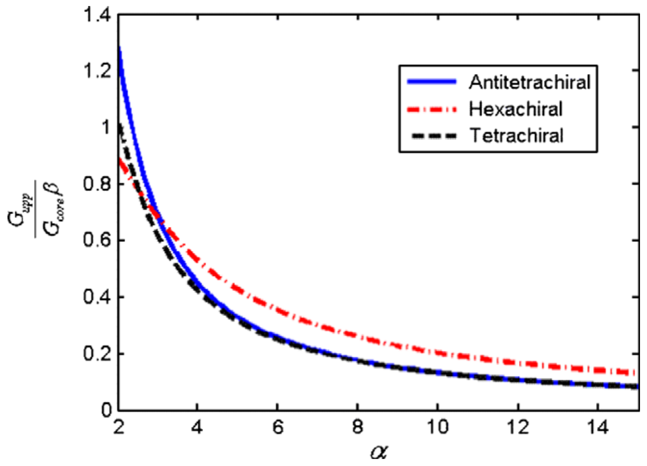

Fig. 5. Nondimensional Voigt bounds for antitetrachiral, hexa and tetrachiral configurations.

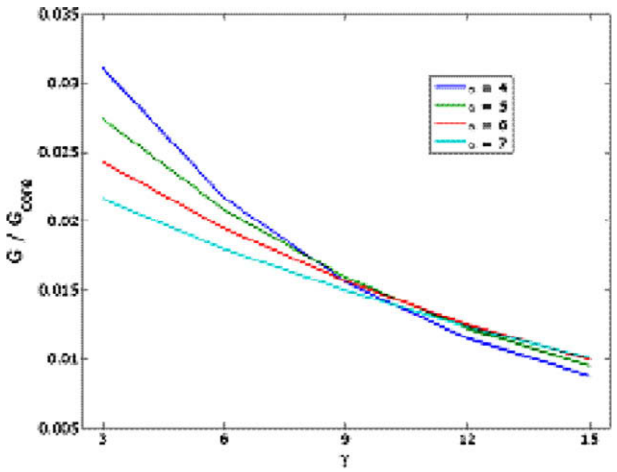

Fig. 6. Nondimensional Voigt bound for tetrachiral configurations for various α ($\beta = 0.05$).

$$\frac{G_{low}}{G_{core}\beta} \cong \alpha \frac{k_1}{1+\alpha \cdot k_2} \tag{18}$$

where $k_1 = 0.045$ and $k_2 = 0.67$ for the tetrachiral cases, and $k_1 = 0.045$, $k_2 = 0.23$ for the hexachiral one. For the Voigt bound, the hexachiral configuration provides consistently higher values than the tetrachiral ones. A unique value for the transverse shear modulus depending on the gauge thickness can be calculated using an approach similar to the one of Grediac [26] and refined for auxetic centresymmetric configurations by Scarpa and Tomlin [27]. After a NLLS procedure on 200 samples similar to the one performed for the estimation of the Reuss bound, the transverse shear modulus can therefore be expressed as:

$$G = G_{low} + \frac{K}{\gamma}(G_{up} - G_{low}) \tag{19}$$

where K is 1.35 for hexachiral configurations, and 1.57 for the tetrachiral ones. It is worth noticing that the analogous value of K for re-entrant auxetic honeycombs [27] is 1.34.

Fig. 7 shows a plot of the non-dimensional transverse shear modulus $G/\beta/G_{core}$ against α for the hexachiral, tetrachiral and both trichiral and antitrichiral configurations generated by FE. As is the case for the in-plane plots for these honeycombs [23], the modulus decreases as the number of ribs attached to each node decreases.

Table 3 shows a comparison between the FE and experimental results related to the four sets of hexachiral and tetrachiral samples, together with the estimation of their upper and lower bounds. A convergence test was carried out. The tests were small strain, thus meaning that there should not be any non-linear effects in the deflection. The agreement is generally good, with the antitetrachiral SLS sample 1 and tetrachiral FDM sample providing percentage error between 7.1% and 7.8%. The second antitetrachiral sample shows a percentage error of 10.7%, while the FDM hexachiral has a slightly larger error of 14.4%. For all cases, the experimental results have a higher magnitude compared to the one provided by the models which could be due to material variations. The interpolation from Eq. (21) gives a satisfactory agreement with the experimental and FE results (12% and 18% of discrepancy with the experiments for the FDM samples), although the interpolated transverse shear modulus offers a conservative estimation. For the samples with the higher relative density (antitetrachiral SLS), the discrepancy is significantly higher, with 23% and 50% for the antitetrachiral samples 1 and 2. Sample 2, in particular, shows a very high experimental shear modulus, anomaly close to the theoretical Voigt bound for the particular gauge aspect ratio considered ($\gamma = 6.3$). Table 1 shows the comparison for the trichiral configurations between FE and experimental results and good agreement is shown. While a more significant discrepancy exists for the honeycombs with the highest relative density ($\beta = 0.4$), a very satisfactory concurrence can be recorded for the thinner honeycombs, with errors around the 5% level.

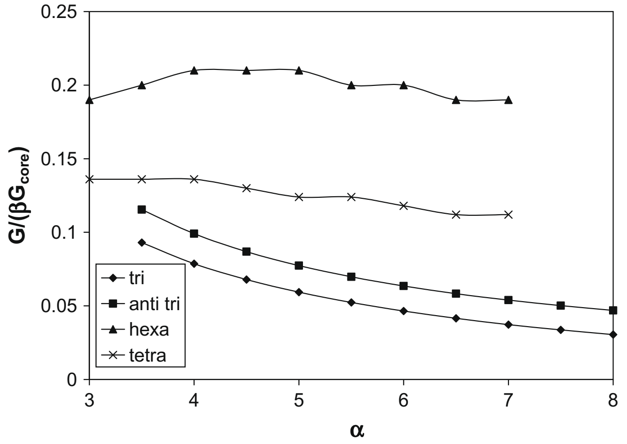

Fig. 7. $G/(\beta G_{core})$ vs. α ($\gamma = 5$, $\beta = 0.05$) for hexachiral, tetrachiral, antitrichiral and trichiral configurations generated by FE.

Fig. 8 shows the transverse shear modulus data of Fig. 7 re-plotted as G/G_{core} vs. relative density (ρ/ρ_{core}) calculated using Eqs. (7a)–(7e) with a least squares fit line to each data set. Interestingly, the shear modulus is predicted to be highly density dependent for the 3-coordinated systems (shear modulus increasing with increasing density) whereas it is largely insensitive to density variations for the 6-coordinated system over the same range of α ($3 < \alpha < 7$). At low density the trichiral system has lower transverse shear modulus than the antitrichiral system. However, at $\rho/\rho_{core} = 0.026$ these two systems have the same shear modulus and linear extrapolation of the trichiral data to higher density (i.e. $\alpha < 3.5$) would indicate a higher shear modulus for the trichiral honeycomb with respect to the antitrichiral honeycomb for $\rho/\rho_{core} > 0.026$. Indeed such an extrapolation would also indicate the 3-connected systems have similar transverse shear modulus values as the hexachiral system at $\rho/\rho_{core} \sim 0.05$.

Previous work [15] has benchmarked the hexachiral configurations with both the re-entrant and traditional hexagonal configurations in terms of local and global buckling. In this case, chiral topologies require higher local buckling loads, thus providing an improvement in behaviour for the same relative density and therefore weight of structure [15].

Table 3
Comparison of numerical, experimental and analytical results for shear modulus of 4 and 6 connectivity chiral honeycombs.

	Sample geometry	FE (MPa)	Experimental (MPa)	Voigt bound (MPa)	Reuss bound (MPa)	Interpolated (MPa)
Antitetrachiral SLS sample 1	$r = 4$ mm $\alpha = 5.4$ $\beta = 0.5$ $\gamma = 6.3$	48.4	52.5	97.7	20.9	40.3
Antitetrachiral SLS sample 2	$r = 4.25$ mm $\alpha = 6.2$ $\beta = 0.35$ $\gamma = 11.8$	44.8	50.2	54.4	15.1	25.0
Tetrachiral FDM	$r = 5$ mm $\alpha = 5.0$ $\beta = 0.12$ $\gamma = 10$	7.9	8.5	21.5	4.9	7.5
Hexachiral FDM	$r = 6$ mm $\alpha = 4$ $\beta = 0.10$ $\gamma = 5.9$	10.1	11.8	21.6	6.0	9.6

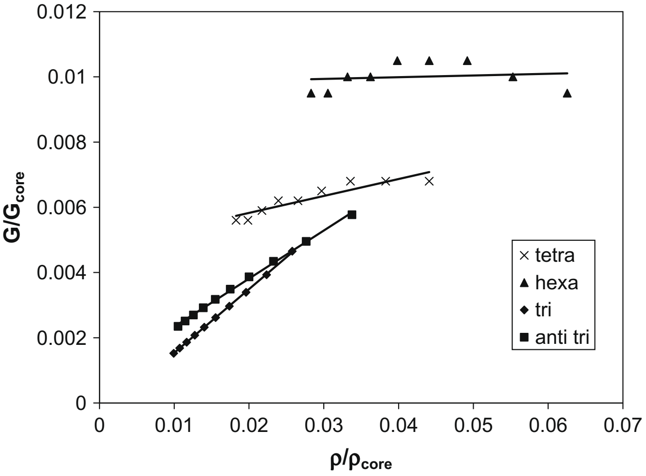

Fig. 8. G/G_{core} vs. ρ/ρ_{core} (γ = 5, β = 0.05) for hexachiral, tetrachiral, antitrichiral and trichiral configurations generated by FE.

5. Conclusions

The out-of-plane linear elastic properties of hexachiral, tetrachiral and trichiral honeycombs have been investigated using analytical, finite element and experimental results. All the different types of honeycombs show an overall sensitivity to cell wall aspect ratios, relative density and gauge thickness similar to the one of hexagonal centresymmetric honeycombs. However, the chiral honeycombs show two distinct upper and lower bounds for the different connectivities, while regular hexagonal honeycombs have coincident bounds. Hexachiral and tetrachiral configurations are also more sensitive to the gauge thickness dependence, while trichiral honeycombs tend to have a lower Voigt and Reuss bound mismatch, and converge to a common shear value after 5–6 non-dimensional γ parameters. For applications where low weight is important (e.g. aerospace sandwich panel components) then it is clear that the higher connectivity honeycombs offer superior transverse shear modulus response than the lower connectivity honeycombs.

Acknowledgement

This work has been funded by the FP6 Project NMP3-CT-2005-013641 – CHISMACOMB.

References

[1] Bitzer T. Honeycomb technology. London: Chapman & Hall; 1997.
[2] Wadley HNG. Multifunctional periodic cellular metals. Philos Trans Roy Soc 2006;A 364:31–68.
[3] Evans KE. Design of doubly curved sandwich panels with honeycomb cores. Comp Struct 1991;17:95–111.
[4] Caddock BD, Evans KE, Masters IG. Honeycomb cores with a negative Poisson's ratio for use in composite sandwich panels. In: Proceedings of the ICCM/8, Honolulu; 1991 [Sections 1–11, 3-E].
[5] Baughman RH, Stafström S, Cui CX, Dantas SO. Materials with negative compressibilities in one or more dimensions. Science 1998;279:1522–4.
[6] Lakes R. Foam structures with negative Poisson's ratio. Science 1987;235:1038–40.
[7] Williams JL, Lewis JL. Properties and an anisotropic model of cancellous bone from the proximal tibia1 epiphysis. J Biomech Eng 1982;104:50–6.
[8] He C, Liu P, Griffin AC, Smith CW, Evans KE. Morphology and deformation behaviour of a liquid crystalline polymer containing laterally attached pentaphenyl rods. Macr Mol Chem Phys 2005;206(2):233–9.
[9] Lakes RS. Advances in negative Poisson's ratio materials. Adv Mater 1993;5:293–6.
[10] Alderson A, Alderson KL. Auxetic Materials Proc Inst Mech Eng Part G. J Aerospace Eng 2007;221:565–75.
[11] Yang W, Li Z-M, Shi W, Xie B-H, Yang M-B. Review on Auxetic materials. J Mater Sci 2004;39(10):3269–79.
[12] Gibson LJ, Ashby MF. Cellular solids: structure and properties. 2nd ed. Cambridge: Cambridge Press; 1997.
[13] Lakes R. Deformation mechanisms in negative Poisson's ratio materials – structural aspects. J Mater Sci 1991;26:2287–92.
[14] Prall D, Lakes R. Properties of a chiral honeycomb with a Poisson's ratio – 1. Int J Mech Sci 1996;39:305–14.
[15] Spadoni A, Ruzzene M, Scarpa F. Global and local linear buckling behaviour of a chiral cellular structure. Phys Status Solidi B 2005;242(3):695–709.
[16] Scarpa F, Blain S, Lew T, Perrott D, Ruzzene M, Yates JR. Elastic buckling of hexagonal chiral cell honeycombs. Composites Part A 2007;38(2):280–9.
[17] Spadoni A, Ruzzene M. Structural and acoustic behavior of chiral truss-core beams. J Vib Acous 2006;128(5):616–26.
[18] Smith CW, Grima JN, Evans KE. A novel mechanism for generating auxetic behaviour in reticulated foams: missing rib foam model. Acta Mater 2000;48(17):4349–56.
[19] Grima JN, Gatt R, Farrugia PS. On the properties of auxetic meta-tetrachiral structures. Phys Status Solidi B 2008;245(3):511–20.
[20] Gaspar N, Ren XJ, Smith CW, Grima JN, Evans KE. Novel honeycombs with auxetic behaviour. Acta Mater 2005;53(8):2439–45.
[21] Wojciechowski KW. Two-dimensional isotropic systems with a negative Poisson ratio. Phys Lett 1989;A137:60–4.
[22] Paulhac A, Perrott D, Scarpa F, Yates J. Transverse shear strength of chiral cellular core. In: ICEM12 conference proceedings, Bari, Italy, 29 August–2 September 2004.
[23] Alderson A, Alderson KL, Attard D, Evans KE, Gatt R, Grima JN, et al. Elastic constants of 3-, 4- and 6- connected chiral and antichiral honeycombs subject to uniaxial in-plane loading. Compos Sci Tech, this issue, doi:10.1016/j.compscitech.2009.07.009.
[24] ABAQUS 6.7-1, 2007, Dassault Systèmes, F.
[25] ANSYS 11.0, ANSYS Inc., Canonsburg, PA.
[26] Grediac M. A finite element study of the transverse shear in honeycomb cores. Int J Solids Struct 1993;30(13):1777–88.
[27] Scarpa F, Tomlin PJ. On the transverse shear modulus of negative Poisson's ratio honeycomb structures. Fatigue Fract Eng Mater Struct 2000;23:717–20.